

Research



**Cite this article:** Nassar H, Chen H, Norris AN, Haberman MR, Huang GL. 2017 Non-reciprocal wave propagation in modulated elastic metamaterials. *Proc. R. Soc. A* **473**: 20170188. <http://dx.doi.org/10.1098/rspa.2017.0188>

Received: 16 March 2017

Accepted: 1 June 2017

**Subject Areas:**  
mechanical engineering

**Keywords:**  
non-reciprocity, pump wave, one-way transition, unidirectional bandgap

**Author for correspondence:**  
G. L. Huang  
e-mail: [huangg@missouri.edu](mailto:huangg@missouri.edu)

# Non-reciprocal wave propagation in modulated elastic metamaterials

H. Nassar<sup>1</sup>, H. Chen<sup>1</sup>, A. N. Norris<sup>2</sup>, M. R. Haberman<sup>3</sup>  
and G. L. Huang<sup>1</sup>

<sup>1</sup>Department of Mechanical and Aerospace Engineering, University of Missouri, Columbia, MO 65211, USA

<sup>2</sup>Department of Mechanical and Aerospace Engineering, Rutgers University, Piscataway, NJ 08854-8058, USA

<sup>3</sup>Department of Mechanical Engineering and Applied Research Laboratories, The University of Texas at Austin, Austin, TX 78712, USA

ID HN, 0000-0001-7235-4498; GLH, 0000-0002-6238-6127

Time-reversal symmetry for elastic wave propagation breaks down in a resonant mass-in-mass lattice whose inner-stiffness is weakly modulated in space and in time in a wave-like fashion. Specifically, one-way wave transmission, conversion and amplification as well as unidirectional wave blocking are demonstrated analytically through an asymptotic analysis based on coupled mode theory and numerically thanks to a series of simulations in harmonic and transient regimes. High-amplitude modulations are then explored in the homogenization limit where a non-standard effective mass operator is recovered and shown to take negative values over unusually large frequency bands. These modulated metamaterials, which exhibit either non-reciprocal behaviours or non-standard effective mass operators, offer promise for applications in the field of elastic wave control in general and in one-way conversion/amplification in particular.

## 1. Introduction

Resonant spring-mass lattices have been studied for at least a century now since they were first introduced by Lord Kelvin in the late 1800s in an attempt to explain dispersion for optical waves [1]. It is not until recently, however, that they have been implemented as subwavelength compact mechanical filters by Liu *et al.* [2] in a mass-in-mass design using

silicon-rubber-coated lead spheres stacked in an epoxy matrix. The renewed recognition of local resonances as a powerful mechanism for the generation of bandgaps has effectively opened up a new major thrust in acoustic and elastic metamaterials research (e.g. [3–8]).

In particular, metamaterials with broken time-reversal symmetry and reciprocity constitute a growing area of interest as they have proved vital for achieving non-reciprocal wave control. In a medium where time-reversal symmetry is not observed, identical wave forms incident in opposite directions can be transformed differently. This phenomenon offers new possibilities in selective wave control as it increases the set of variables based on which waves can be segregated: their frequency, polarization, direction and, thanks to non-reciprocity, the sign of their group velocity. Examples of applications include the realization of directional mode converters [9–11], selective acoustic circulators [12], directional wave reflectors [13,14] and directional wave accelerators [15].

A lossy material, where energy is irreversibly dissipated, is an example of a system without time-reversal symmetry. More interestingly, media including strongly nonlinear components or featuring specific chiral microstructures can have a diode effect on acoustic wave propagation either in the bulk of the medium or along its edges [16–19]. These configurations can be qualified as intrinsic since they do not feature any external stimuli. By contrast, in extrinsic configurations, the breaking of time-reversal symmetry is the consequence of an externally applied loading either in the form of a biasing distribution of angular momenta [12,20–23] or in the form of a ‘pump wave’. In the latter case, a pump wave is the name given to a wave-like space–time modulation of the constitutive properties of a host medium. By changing, say, the elastic stiffness of the medium in space and in time, a bias breaking time-reversal symmetry can be introduced. The scattering of travelling elastic waves by a pump wave has been examined in connection with parametric amplification in the previous century by many authors [24–29] and subsequently in the context of ‘dynamic materials’ by Lurie [30] and co-workers (see also [31] and references therein). Finally, evidence for one-way mode transitions and one-directional bandgaps in weakly modulated waveguides were advanced by Yu & Fan [9] and Zanjani *et al.* [10,11] on one hand and by Swinteck *et al.* [13] and Trainiti & Ruzzene [14] on the other hand. Here, we build on their work and show how weakly modulated resonant metamaterials offer both possibilities simultaneously.

The present paper aims to characterize wave propagation in a resonant metamaterial where the inner stiffness is weakly modulated in a wave-like fashion. It is demonstrated both analytically and numerically that the dispersive two-branch nature of the band diagram of the metamaterial combined with the loss of time-reversal symmetry offers a rich wave control potential including selective one-way conversion/transmission and reflection. Note that as suggested by Casadei *et al.* [32] and Chen *et al.* [33,34], modulating the inner stiffness of a metamaterial is technologically feasible using programmable piezoelectric components. Other techniques for guiding pump waves can make use of shock waves in soft materials [35], of magnetic fields soliciting magneto-rheological elastomers [36] or of the photo-elastic effect [13,37].

Furthermore, beyond symmetry breaking, we explore a set of strong space–time modulations that turn out to have a significant impact on the behaviour of the effective mass operator in the homogenization limit. As a matter of fact, in addition to the main bandgap of the inner-resonant metamaterial, a set of secondary bandgaps appear at low frequencies. Most importantly, modulation-induced bandgaps are proved to be able to merge together into broader gaps in contrast to what is systematically observed at low frequencies in non-modulated metamaterials (e.g. [4]).

The rest of the paper goes as follows. Section 2 is a brief reformulation of known results on non-modulated mass-in-mass metamaterials. In §3, we derive the first-order asymptotics for the dispersion curve of a weakly modulated metamaterial using coupled mode theory. It is shown that a pump wave couples various free waves propagating through the metamaterial as soon as they satisfy a phase matching condition. Depending on the sign of the involved group velocities, the coupling will be termed ‘veering’ (co-directional coupling) leading to one-way mode conversion or will be termed ‘locking’ (contra-directional coupling) leading to one-directional bandgaps. A quantitative and qualitative analysis of these phenomena based on

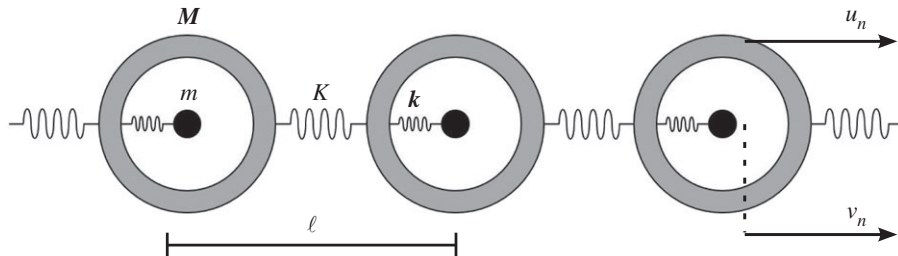


**Figure 1.** A discrete spring mass-in-mass metamaterial.

our analytical findings and a series of numerical experiments is presented. Section 4 is a limit case study describing the behaviour of the metamaterial under strong extremely short-wavelength modulations. Finally, concluding remarks are presented in §5.

## 2. Wave propagation in non-modulated elastic metamaterials

We start by characterizing free and forced wave propagation in non-modulated inner-resonant metamaterials. The results will serve as a theoretical basis for the next section where we deal with modulated metamaterials.

### (a) Discrete and continuous modelling of a metamaterial

A well-known model for inner-resonant metamaterials is the discrete spring mass-in-mass lattice depicted in figure 1 (see [1], for a brief historical account). The outer rigid shells have mass  $M$  and are connected by linear springs of constant  $K$ . The inner resonators have mass  $m$  and are connected to outer masses through springs of constant  $k$ . The motion equations read

$$\left. \begin{aligned} M\partial_t^2 u_n &= -k(u_n - v_n) + K(u_{n+1} + u_{n-1} - 2u_n) \\ m\partial_t^2 v_n &= -k(v_n - u_n), \end{aligned} \right\} \quad (2.1)$$

and

where  $u_n \equiv u_n(t)$  and  $v_n \equiv v_n(t)$  denote the displacement of the  $n$ th outer and inner masses, respectively, and  $\partial_t^2$  indicates differentiating with respect to time  $t$ , twice. When the frequency  $\omega$  of the propagating waves is significantly smaller than the phononic cut-off frequency  $2\sqrt{K/M}$ , a continuous counterpart to the above discrete motion equations exists and can be written as

$$\left. \begin{aligned} M\partial_t^2 u &= -k(u - v) + E\partial_x^2 u \\ m\partial_t^2 v &= -k(v - u), \end{aligned} \right\} \quad (2.2)$$

and

where  $\partial_x$  is the space derivative. The displacements  $u$  and  $v$  are now functions of the continuous space variable  $x$  and of time  $t$ . The coefficient  $E = K\ell^2$  can be identified as the elastic stiffness of the master structure,  $\ell$  being the spacing between the centres of two consecutive outer masses.

Unlike earlier studies such as the one by Brillouin [1], recent papers investigate the properties of the considered metamaterial through the mean of an effective mass density operator first introduced by Auriault & Bonnet [38] in the more general context of stiff-matrix soft-inclusions elastodynamics. Here, since  $k$  will be subject to space-time modulations, the effective mass density cannot be as easily defined and the present multi-displacement approach is preferred (e.g. [39]).

It is also helpful to combine the motion equations into a single governing equation using matrices. Thus, let

$$M = \begin{bmatrix} M & 0 \\ 0 & m \end{bmatrix}, \quad E = \begin{bmatrix} E & 0 \\ 0 & 0 \end{bmatrix}, \quad k = \begin{bmatrix} k & -k \\ -k & k \end{bmatrix} \quad \text{and} \quad \psi = \begin{bmatrix} u \\ v \end{bmatrix}. \quad (2.3)$$

Given these matrix notations, the governing equations can be grouped into

$$M\partial_t^2\psi = -k\psi + E\partial_x^2\psi. \quad (2.4)$$

## (b) Free and forced wave propagation

Plane harmonic waves

$$\psi(x, t) = \Psi e^{i(qx - \omega t)} \quad (2.5)$$

of wavenumber  $q$ , frequency  $\omega$  and amplitude  $\Psi$  can travel through a homogeneous metamaterial upon satisfying

$$(-\omega^2 M + k + q^2 E)\Psi = 0. \quad (2.6)$$

This eigenvalue problem admits non-trivial solutions when the dispersion relation  $\det(-\omega^2 M + k + q^2 E) = 0$  is satisfied, an equivalent form of which is

$$D(\omega, q) \equiv E q^2 - \omega^2 \left( M + m \frac{\Omega^2}{\Omega^2 - \omega^2} \right) = 0, \quad (2.7)$$

with  $\Omega = \sqrt{k/m}$  being the resonance frequency of the inner masses.

A solution  $(q, \omega)$  to equation (2.7) is hereafter referred to as an eigenmode. The corresponding amplitude is denoted  $\Psi_{q,\omega}$  and is called an eigenvector. Also, we will call eigenstate the combination of an eigenmode and an eigenvector, as well as the corresponding free wave. The equation of motion (2.2)<sub>2</sub> for the resonators implies that the eigenvectors can be defined as

$$\Psi_{q,\omega} = \Psi_\omega = \begin{bmatrix} U \\ V \end{bmatrix} = \begin{bmatrix} k - \omega^2 m \\ k \end{bmatrix}. \quad (2.8)$$

In conclusion, a free wave propagating through a homogeneous metamaterial is a superposition of plane harmonic waves  $\Psi_\omega e^{i(qx - \omega t)}$ , where  $(q, \omega)$  is an eigenmode solution to equation (2.7).

Now, it is assumed that the metamaterial is subjected to a harmonic plane wave body force of wavenumber  $q$ , frequency  $\omega$  and amplitude  $F$ . The motion equation becomes

$$M\partial_t^2\psi = -k\psi + E\partial_x^2\psi + F e^{i(qx - \omega t)}. \quad (2.9)$$

When  $(q, \omega)$  is not an eigenmode,  $F$  will always drive  $\psi$  into bounded oscillations of the same frequency  $\omega$  and wavenumber  $q$  and of amplitude  $\Psi = (-\omega^2 M + k + q^2 E)^{-1}F$ . By contrast, when  $(q, \omega)$  is an eigenmode,  $F$  will cause  $\psi$  to have oscillations of increasing and unbounded amplitude unless  $F$  was orthogonal to  $\Psi_\omega$ . In general,

$$(-\omega^2 M + k + q^2 E)\Psi = F \quad (2.10)$$

necessarily implies the secular condition

$$\Psi_\omega \cdot F = \Psi_\omega \cdot (-\omega^2 M + k + q^2 E)\Psi = 0, \quad (2.11)$$

thanks to the symmetry of  $M$ ,  $E$  and  $k$ . This orthogonality property will provide essential information on wave dispersion in modulated metamaterials.

## 3. Wave propagation in modulated elastic metamaterials

Wave-like modulations of the metamaterial are first introduced. A perturbative approach based on the amplitude of the modulation then offers an efficient way to understand, to leading order, how an incident wave is transformed, converted and transmitted by the modulation. The constructed wave solutions demonstrate non-reciprocal directional behaviour by which waves travelling in one direction are either blocked or converted in a different manner than waves travelling in the opposite direction.

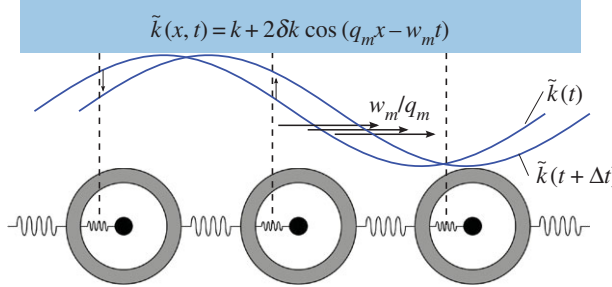


**Figure 2.** An illustration of a modulated metamaterial. The sinusoidal modulation travels at a uniform speed  $\omega_m/q_m$ . (Online version in colour.)

### (a) Wave-like modulations

Using programmable piezoelectric active components for instance [32–34], it is possible to control the value of the coupling stiffness  $k$  and to modulate it in space and in time in a wave-like periodic fashion (figure 2). Thus, let

$$\tilde{k} = \tilde{k}(x, t) = \tilde{k}(q_m x - \omega_m t) \quad (3.1)$$

be the modulated stiffness and be a  $2\pi$ -periodic function of the phase  $q_m x - \omega_m t$ . In what follows, we assume that the difference between the modulated stiffness  $\tilde{k}$  and its average value  $k$  remains small. Furthermore, the profile of  $\tilde{k}$  is taken to be sinusoidal. In summary, the modulation takes the form of a harmonic plane wave of wavenumber  $q_m$  and frequency  $\omega_m$  and has the expression

$$\tilde{k}(x, t) = k + 2\delta k(x, t) = k + 2\delta k \cos(q_m x - \omega_m t), \quad (3.2)$$

where  $\delta k$  is small compared with  $k$ .

This choice is motivated by two facts. First, studying low-amplitude modulations allows to understand the continuous transition between a non-modulated ( $\delta k = 0$ ) and a modulated ( $0 \neq \delta k \ll k$ ) metamaterial, and consequently how non-reciprocity gradually starts manifesting. Second, weakly modulated media will prove to exhibit a directional wave-conversion potential that has no counterpart in strongly modulated media thus extending the results obtained by Yu & Fan [9] and by Zanjani *et al.* [10,11] to inner-resonant metamaterials.

Calling  $\tilde{\psi}$  the displacement field in the modulated metamaterial, the motion equation becomes

$$M\partial_t^2 \tilde{\psi} = -\tilde{k}\tilde{\psi} + E\partial_x^2 \tilde{\psi}, \quad (3.3)$$

with

$$\tilde{k}(x, t) = k + 2\delta k(x, t) = k + 2\delta k \cos(q_m x - \omega_m t). \quad (3.4)$$

As all coefficients are either constant or periodic,  $\tilde{\psi}$  decomposes into a superposition of Floquet–Bloch waves

$$\tilde{\psi}(x, t) = \tilde{\Psi}(q_m x - \omega_m t) e^{i(\tilde{q}x - \tilde{\omega}t)} \quad (3.5)$$

of wavenumber  $\tilde{q}$  and frequency  $\tilde{\omega}$ , where  $\tilde{\Psi}$  is  $2\pi$ -periodic just like the modulation.

### (b) Perturbation method

Taking advantage of the smallness of  $\delta k$ , we look for solutions in the perturbed form

$$\tilde{\Psi} = \Psi + \delta\Psi + \dots, \quad \tilde{q} = q + \delta q + \dots \quad \text{and} \quad \tilde{\omega} = \omega + \delta\omega + \dots \quad (3.6)$$

where  $\delta\Psi$ ,  $\delta q$  and  $\delta\omega$  are first-order corrections to  $\Psi$ ,  $q$  and  $\omega$ , respectively, and are all of the same order of magnitude as the modulation amplitude  $\delta k$ . Our purpose is to calculate the amplitude  $\tilde{\Psi}$  to leading order, i.e.  $\Psi$ , and to determine how the first-order corrections ( $\delta q, \delta\omega$ ) modify the dispersion curve.

Let  $\xi$  be the non-dimensional phase variable

$$\xi = q_m x - \omega_m t. \quad (3.7)$$

Injecting (3.6) and (3.5) into (3.3) yields to leading order

$$M(-i\omega - \omega_m \partial_\xi)^2 \Psi = -k\Psi + E(iq + q_m \partial_\xi)^2 \Psi. \quad (3.8)$$

Recalling that  $\Psi$  is a  $2\pi$ -periodic function of  $\xi$ , it can be expanded into a Fourier series

$$\Psi(\xi) = \sum_{j \in \mathbb{Z}} \Psi^j e^{ij\xi}, \quad (3.9)$$

where the constant amplitudes  $\Psi^j$  are solutions to the algebraic eigenvalue problem

$$[-(\omega + j\omega_m)^2 M + k + (q + jq_m)^2 E] \Psi^j = 0. \quad (3.10)$$

Now, for  $\Psi$  to exist and be non-zero, one of the Fourier coefficients  $\Psi^j$  must exist and also be non-zero. Accordingly, there exists at least one integer  $j$  such that  $(q + jq_m, \omega + j\omega_m)$  is an eigenmode solution to equation (2.7). Call  $J$  the set of all such indices. By a harmless phase change and without loss of generality, it is possible to ensure that  $0 \in J$ . In other words,  $(q, \omega)$  is an eigenmode and we can write

$$\Psi(\xi) = \Psi^0 + \sum_{j \in J - \{0\}} \Psi^j e^{ij\xi} \quad (3.11)$$

where  $\Psi^j$  are eigenvectors associated with the eigenmodes  $(q + jq_m, \omega + j\omega_m)$ , for  $j \in J$ . Finally, with the notations of the previous section, we recover

$$\Psi(\xi) = V^0 \Psi_\omega + \sum_{j \in J - \{0\}} V^j \Psi_{\omega_j} e^{ij\xi}, \quad (3.12)$$

with  $\omega_j = \omega + j\omega_m$ . For later use, we similarly define  $q_j = q + jq_m$ .

Physically speaking,  $\Psi_\omega$  is interpreted as an incident wave and the  $\Psi_{\omega_j}$  are seen as scattered, or reflected waves generated by the modulation. Two eigenstates  $(q, \omega)$  and  $(q', \omega')$  are therefore coupled, i.e. can be identified as a pair of incident and scattered waves, whenever there exists an integer  $j$  such that the phase matching condition

$$q' - q = jq_m \quad \text{and} \quad \omega' - \omega = j\omega_m \quad (3.13)$$

is satisfied. Subsequent calculations will in fact show that  $j$  must be equal to  $\pm 1$  for the coupling to take place. In general, when the pump wave has its first  $N$  Fourier components non-zero,  $j$  can take integer values between  $-N$  and  $N$  (see equation (3.29)).

A graphical illustration can help identifying pairs of coupled modes (figure 3). Starting with the dispersion curve of the non-modulated metamaterial  $\mathcal{C} = \mathcal{C}^0$ , we plot the translated curves  $\mathcal{C}^j = \mathcal{C} - (jq_m, j\omega_m)$ ,  $j = \pm 1$ . Points of no-intersection of  $\mathcal{C}$  correspond to cases where  $(q, \omega)$  is the only eigenmode among the  $(q_j, \omega_j)$  so that

$$\Psi(\xi) = V^0 \Psi_\omega \quad (3.14)$$

is composed of a single uncoupled mode: the incident wave. Here, the metamaterial appears transparent and no scattered waves are generated. Points of intersection  $\mathcal{C} \cap \mathcal{C}^j$  on the other hand correspond to cases where both  $(q, \omega)$  and  $(q_j, \omega_j)$  are eigenmodes. Hence,

$$\Psi(\xi) = V^0 \Psi_\omega + V^j \Psi_{\omega_j} e^{ij\xi} \quad (3.15)$$

is the sum of a pair of coupled modes, one incident and one scattered. On the example of figure 3, there appears to be three such intersection pairs labelled as  $A$ ,  $B$  and  $C$ : when one 'leg' of a given pair is incident, the other 'leg' is scattered and vice versa. Last, we exclude rare cases where more than two curves intersect at a single point.

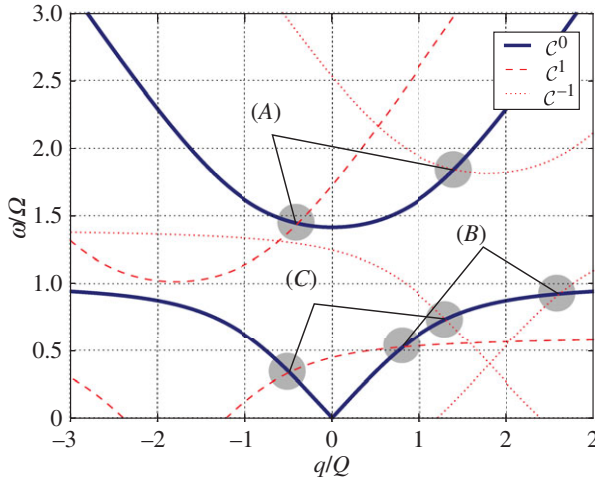


**Figure 3.** Coupling and non-reciprocity: the pairs of coupled modes  $A$ ,  $B$  and  $C$  are pinned. Notice that they are non-symmetrically distributed, a symptom of the breaking of time-reversal symmetry. The normalizing wavenumber is  $Q = \sqrt{k/E} = \sqrt{k/K/\ell}$ . For this illustration, we used  $m/M = 1$ ,  $q_m/Q = 1.8$  and  $\omega_m/\Omega = 0.4$ . (Online version in colour.)

Note that non-reciprocity is already at play here since, generally speaking, when a pair of eigenstates  $(q, \omega)$  and  $(q_j, \omega_j)$  are coupled, their counterparts propagating in the opposite directions, i.e.  $(-q, \omega)$  and  $(-q_j, \omega_j)$  are not coupled. In other words, if the eigenstate  $(q, \omega)$  is scattered if incident in one direction, it will not be scattered when incident in the opposite direction. Graphically, this corresponds to the loss of parity in the plot of figure 3.

### (c) Uncoupled modes

Let us assume first that  $(q, \omega)$  is a non-intersection point. Thus,  $\Psi$  takes the form (3.14), and the coefficient  $V^0$  can be chosen arbitrarily by linearity. Regarding the determination of  $\delta q$  and  $\delta\omega$ , combining again (3.3), (3.5) and (3.6) and keeping first-order terms entail

$$[M(i\omega + \omega_m \partial_\xi)^2 - E(iq + q_m \partial_\xi)^2 + k]\delta\Psi = (2\omega\delta\omega M - 2\delta k - 2q\delta q E)\Psi. \quad (3.16)$$

Then,  $\delta\Psi$  propagates through the non-modulated medium under the influence of a modulation-induced body force

$$F = (2\omega\delta\omega M - 2q\delta q E)\Psi - 2\delta k\Psi. \quad (3.17)$$

Averaging with respect to  $\xi$  over a unit cell  $[0, 2\pi]$  simplifies the above equation into

$$(-\omega^2 M + q^2 E + k) \langle \delta\Psi \rangle = (2\omega\delta\omega M - 2q\delta q E)\Psi, \quad (3.18)$$

where we have used the fact that  $\delta\Psi$  is periodic and that  $k$  is the average of  $\tilde{k}$  so that  $\langle \delta k \rangle = 0$ . Therein,  $\langle \cdot \rangle \equiv (1/2\pi) \int_0^{2\pi}$  is the averaging operator. As  $(q, \omega)$  is an eigenmode, the orthogonality condition

$$\Psi_\omega \cdot (2\omega\delta\omega M - 2q\delta q E)\Psi = 0 \quad (3.19)$$

holds. As a consequence, by using (3.14), we obtain

$$\Psi_\omega \cdot (2\omega\delta\omega M - 2q\delta q E)\Psi_\omega = 0. \quad (3.20)$$

This condition is equivalent to a variation of the dispersion relation (2.7),

$$\frac{\partial D}{\partial \omega} \delta\omega + \frac{\partial D}{\partial q} \delta q = 0 \quad \Leftrightarrow \quad \delta\omega = c\delta q, \quad (3.21)$$

where  $c$  is the group velocity,

$$c(\omega, q) = -\frac{\partial D}{\partial q} \Bigg/ \frac{\partial D}{\partial \omega} = \frac{qE(\Omega^2 - \omega^2)^2}{\omega(M(\Omega^2 - \omega^2)^2 + m\Omega^4)}. \quad (3.22)$$

In other words, the frequency and wavenumber remain on the non-modulated dispersion curve  $\mathcal{C}^0$  of the non-modulated medium for any permissible change  $\delta\omega, \delta q$ . The group speed relation also implies that  $\delta\omega$  vanishes whenever  $\delta q$  does. This means that an incident wave of a given frequency  $\omega$  propagates with the same wavenumber  $\tilde{q} = q$ , to first order, in both the modulated and the non-modulated metamaterials. Accordingly, to first order, introducing a wave-like modulation does not alter the dispersion curve in the vicinity of non-coupled modes.

#### (d) Coupled modes

When  $(q, \omega)$  coincides with an eigenmode that is an intersection point  $(q_0, \omega_0)$ , there exists a non-zero integer  $j$  such that  $(q_j, \omega_j)$  is an eigenmode as well. We say that the modes  $(q_0, \omega_0)$  and  $(q_j, \omega_j)$  are coupled. The amplitude  $\Psi$  now takes the form (3.15) and the first-order motion equation reads

$$\begin{aligned} & [M(i\omega_0 + \omega_m \partial_\xi)^2 - E(iq_0 + q_m \partial_\xi)^2 + k] \delta\Psi(\xi) \\ &= [-2(i\omega_0 + \omega_m \partial_\xi) i\delta\omega M - 2\delta k(\xi) + 2(iq_0 + q_m \partial_\xi) i\delta q E] V^j \Psi_{\omega_j} e^{ij\xi} \\ &\quad + (2\omega_0 \delta\omega M - 2\delta k(\xi) - 2q_0 \delta q E) V^0 \Psi_{\omega_0}. \end{aligned} \quad (3.23)$$

The modulation-induced body force has again to satisfy some orthogonality conditions. To obtain them, consider the average of the above equation over a unit cell:

$$(-\omega_0^2 M + q_0^2 E + k) \langle \delta\Psi(\xi) \rangle = -2\bar{\delta}_j k V^j \Psi_{\omega_j} + (2\omega_0 \delta\omega M - 2q_0 \delta q E) V^0 \Psi_{\omega_0}, \quad (3.24)$$

with a superimposed bar indicating complex conjugation and

$$\delta_j k = \left\langle \delta k e^{-ij\xi} \right\rangle \quad (3.25)$$

being the  $j$ th Fourier coefficient of the modulation  $k$ . Therefore,  $\langle \delta\Psi \rangle$  is excited by a resonating body force at the eigenmode  $(q_0, \omega_0)$  entailing

$$-2V^j \Psi_{\omega_j} \cdot \bar{\delta}_j k \Psi_{\omega_j} + V^0 \Psi_{\omega_0} \cdot (2\omega_0 \delta\omega M - 2q_0 \delta q E) \Psi_{\omega_0} = 0. \quad (3.26)$$

In the same manner, multiplying equation (3.23) by  $e^{-ij\xi}$  and averaging yields a second relationship between  $V^0$  and  $V^j$ . The two equations combined imply that the coefficients  $V^0$  and  $V^j$  form a solution to the eigenvalue problem

$$\begin{bmatrix} \Psi_{\omega_0} \cdot (2\omega_0 \delta\omega M - 2q_0 \delta q E) \Psi_{\omega_0} & -2\Psi_{\omega_0} \cdot \bar{\delta}_j k \Psi_{\omega_j} \\ -2\Psi_{\omega_j} \cdot \delta_j k \Psi_{\omega_0} & \Psi_{\omega_j} \cdot (2\omega_j \delta\omega M - 2q_j \delta q E) \Psi_{\omega_j} \end{bmatrix} \begin{bmatrix} V^0 \\ V^j \end{bmatrix} = \begin{bmatrix} 0 \\ 0 \end{bmatrix}, \quad (3.27)$$

where the involved eigenvectors are explicitly given by equation (2.8).

Forming the inner products and using the result for the uncoupled mode yields

$$\begin{bmatrix} \left( \frac{\delta\omega}{c_0} - \delta q \right) q_0 E(k - m\omega_0^2)^2 & -\bar{\delta}_j k m^2 \omega_0^2 \omega_j^2 \\ -\delta_j k m^2 \omega_0^2 \omega_j^2 & \left( \frac{\delta\omega}{c_j} - \delta q \right) q_j E(k - m\omega_j^2)^2 \end{bmatrix} \begin{bmatrix} V^0 \\ V^j \end{bmatrix} = \begin{bmatrix} 0 \\ 0 \end{bmatrix}, \quad (3.28)$$

where  $c_0 = c(\omega_0, q_0)$  and  $c_j = c(\omega_j, q_j)$  are the group speeds. Finally, the first-order corrections  $(\delta q, \delta\omega)$  to the dispersion curve can be determined by setting the determinant to zero, yielding

$$\left( \delta q - \frac{\delta\omega}{c_0} \right) \left( \delta q - \frac{\delta\omega}{c_j} \right) = \frac{1}{q_0 q_j} \left( \frac{|\delta_j k| m^2 \omega_0^2 \omega_j^2}{E(k - m\omega_0^2)(k - m\omega_j^2)} \right)^2. \quad (3.29)$$

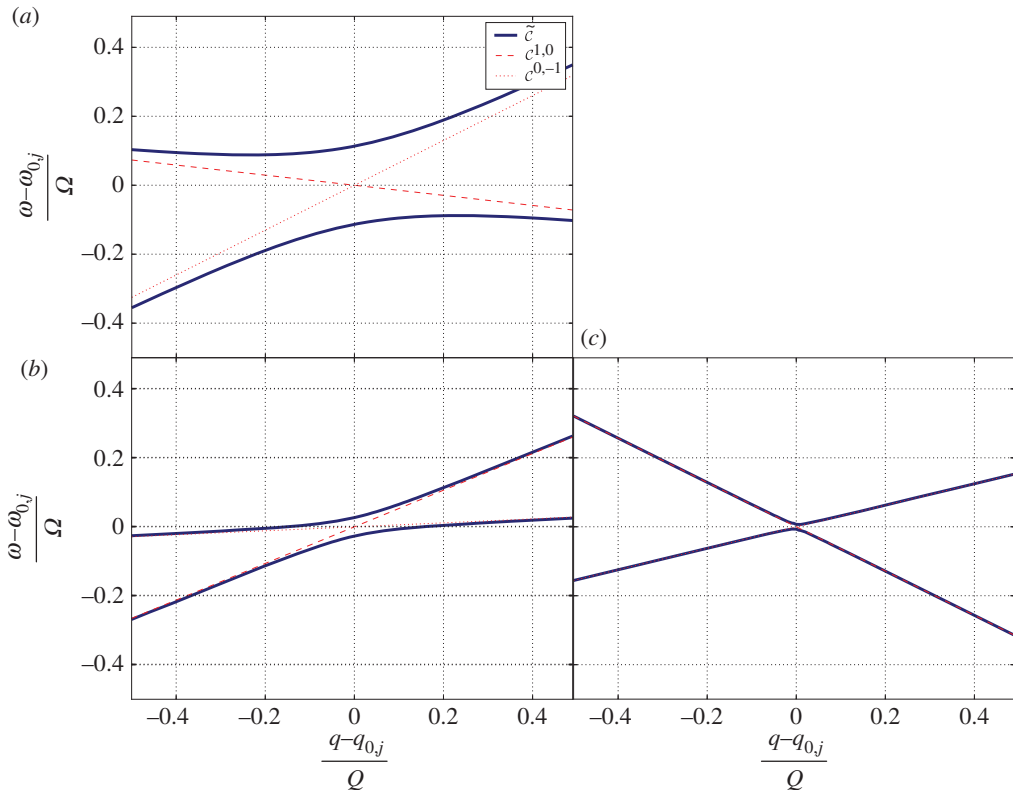


**Figure 4.** First-order corrections to the dispersion curve of a modulated metamaterial in the vicinity of the pairs of coupled modes *a*, *b* and *c* of figure 3. (Online version in colour.)

The resulting dispersion curve can be plotted in two steps. First, use equation (2.7) to plot the dispersion curve everywhere except in the vicinity of the pairs of coupled modes (figure 3). Second, for each pair of coupled modes  $\{(q_0, \omega_0), (q_j, \omega_j)\}$ , obtain  $\delta\omega$  as a function of  $\delta q$  using equation (3.29),

$$\delta\omega = \frac{\delta q}{2}(c_0 + c_j) \pm \sqrt{\left(\frac{\delta q}{2}(c_0 - c_j)\right)^2 + \frac{c_0 c_j}{q_0 q_j} \left(\frac{|\delta_j k| m^2 \omega_0^2 \omega_j^2}{E(k - m\omega_0^2)(k - m\omega_j^2)}\right)^2}, \quad (3.30)$$

and plot both  $\omega_{0,j} + \delta\omega$  as a function of  $q_{0,j} + \delta q$  for  $\delta\omega \ll |\omega_{0,j}|$  and  $\delta q \ll |q_{0,j}|$  (figure 4). The resulting dispersion curve is depicted in figure 5.

It is worth mentioning that the foregoing analysis is valid regardless of the specific profile of  $\delta k(\xi)$ , the coupling between modes  $(q_0, \omega_0)$  and  $(q_j, \omega_j)$  being as strong as the  $j$ th Fourier coefficient  $\delta_j k$  is large. In the illustrations, however,  $\delta k(\xi)$  is sinusoidal and  $j$  takes only the values  $\pm 1$  as mentioned earlier.

In the following, we closely study the behaviour of the modulated metamaterial in the vicinity of a pair of coupled modes in two cases depending on whether the coupled modes have co-directional or contra-directional group velocities. In the vicinity of pair *B* where both modes have positive group velocities, a phenomenon called ‘locking’ occurs, whereas in the vicinity of pairs *A* and *C*, ‘veering’ occurs [40]. In the present context, veering and locking correspond to whether the modulated metamaterial behave as a directional non-reciprocal wave converter/transmitter (pair *B*) or converter/reflector (pairs *A* and *C*).

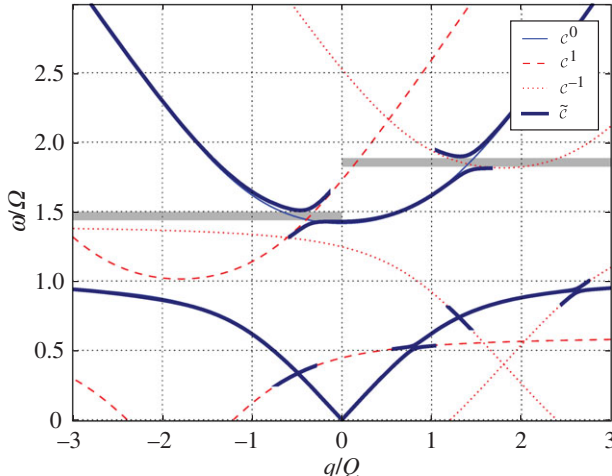


**Figure 5.** The dispersion curve of a modulated metamaterial obtained by combining figures 3 and 4. (Online version in colour.)

It is of interest to underline the fact that veering and associated conversion/reflection phenomena, at the origin of directional bandgaps, can be observed in non-dispersive media such as the standard one-dimensional elastic medium [13,14]. Nonetheless, locking and related conversion/transmission phenomena necessitate the presence of a dispersive host medium such as the metamaterial considered in this paper.

### (e) Directional wave conversion and transmission

Suppose an incident wave has frequency close to the intersection frequency  $\omega_0$ , specifically  $\omega_0 + \delta\omega$ . Equation (3.29) yields the first-order correction to the wavenumbers  $q_0$  and  $q_j$  of the incident and scattered waves. Both are shifted by the two values  $\delta q_+$  and  $\delta q_-$ ,

$$\delta q_{\pm} = \frac{\delta\omega}{2} \left( \frac{1}{c_0} + \frac{1}{c_j} \right) \pm \sqrt{\left( \frac{\delta\omega}{2} \left( \frac{1}{c_0} - \frac{1}{c_j} \right) \right)^2 + \frac{1}{q_0 q_j} \left( \frac{|\delta_j k| m^2 \omega_0^2 \omega_j^2}{E(k - m\omega_0^2)(k - m\omega_j^2)} \right)^2}. \quad (3.31)$$

The associated coupling strengths  $C = V^j/V^0$  can be expressed as

$$C_{\pm} = - \left( \delta q_{\pm} - \frac{\delta\omega}{c_0} \right) \frac{q_0 E(k - m\omega_0^2)^2}{\delta_j k m^2 \omega_0^2 \omega_j^2} = \left( \left( \frac{1}{c_0} - \frac{1}{c_j} \right) \delta\omega \mp (\delta q_+ - \delta q_-) \right) \frac{q_0 E(k - m\omega_0^2)^2}{2 \delta_j k m^2 \omega_0^2 \omega_j^2}. \quad (3.32)$$

Above and in the remainder of this subsection, it is assumed that  $q_0$  and  $q_j$  have the same sign making  $\delta q$  and  $C$  real (e.g. pair B in figure 5).

Having two possible values for  $\delta q$  and  $C$ , the constructed solution  $\psi$  is a superposition of two waves

$$\begin{aligned} \psi(x, t) = & \{ V_+^0 e^{i\delta q_a x} (\Psi_{\omega} e^{i(q_0 x - \omega_0 t)} + (C_a + C_b) \Psi_{\omega_j} e^{i(q_j x - \omega_j t)}) \\ & + V_-^0 e^{-i\delta q_a x} (\Psi_{\omega} e^{i(q_0 x - \omega_0 t)} - (C_a - C_b) \Psi_{\omega_j} e^{i(q_j x - \omega_j t)}) \} e^{i(\delta q_b x - \delta\omega t)}. \end{aligned} \quad (3.32)$$

Here,  $V_{\pm}^0$  correspond to the roots  $\delta q_{\pm}$ , respectively, and for simplicity we have set

$$\delta q_{\pm} = \pm \delta q_a + \delta q_b \quad \text{and} \quad C_{\pm} = \pm C_a + C_b, \quad (3.33)$$

where the specific values of  $\delta q_a$ ,  $\delta q_b$  and  $C_a$ ,  $C_b$  follow from equations (3.31) and (3.32), respectively.

To interpret these results, let us assume that at some position  $x$ , say  $x = 0$ , the only eigenmode present is the one in the vicinity of  $(q_0, \omega_0)$ . This is the case in particular when this eigenmode corresponds to an incident wave that just entered the modulated metamaterial. Therefore, we have  $V_\pm^0 = (C_a \mp C_b)V^0$  so that

$$\begin{aligned} \psi(x, t) = 2V^0 \{ & [(C_a \cos(\delta q_a x) - iC_b \sin(\delta q_a x))\Psi_\omega e^{i(q_0 x - \omega_0 t)} \\ & + i(C_a^2 - C_b^2) \sin(\delta q_a x)\Psi_{\omega_j} e^{i(q_j x - \omega_j t)}] \} e^{i(\delta q_b x - \delta \omega t)}. \end{aligned} \quad (3.34)$$

As  $x$  increases from zero, the amplitude of the initial mode  $(q_0, \omega_0)$  decays until it reaches its minimum amplitude at  $x = d \equiv \pi/(2\delta q_a)$ . This is a consequence of the fact that  $|C_a| \geq |C_b|$  with equality if and only if  $\delta_j k = 0$ , which corresponds to the trivial case of no modulation. At the same time, the amplitude of mode  $(q_j, \omega_j)$  grows from zero, reaching its maximum after propagating through a distance  $d$ . The described modal conversion becomes total when  $C_b = 0$ , which occurs if either  $\delta \omega = 0$  or  $c_0 = c_j$ . The latter possibility is precluded by assumption, and in fact it is clear from figure 3 that the group speeds, i.e. slopes of the curves, are markedly different at the intersection points.

Total mode conversion, therefore, occurs if  $\delta \omega = 0$ , with

$$\delta q_\pm = \pm \frac{|\delta_j k| m^2 \omega_0^2 \omega_j^2}{E |k - \omega_0^2 m| |k - \omega_j^2 m| \sqrt{q_0 q_j}} \quad \text{and} \quad C_\pm = \mp \frac{|k - \omega_0^2 m|}{|k - \omega_j^2 m|} \sqrt{\frac{q_0}{q_j}}. \quad (3.35)$$

In this special case, the incident wave has the precise frequency of mode  $(q_0, \omega_0)$  and, after propagating through a distance  $d = \pi/(2\delta q_+)$ , it will have vanished completely leaving the place for mode  $(q_j, \omega_j)$  that will be the only one present at  $x = d$ . Therefore, a metamaterial modulated through a distance  $d$  converts an incident wave  $V^0 \psi_{\omega_0} e^{i(q_0 x - \omega_0 t)}$  into a wave  $CV^0 \psi_{\omega_j} e^{i(q_j x - \omega_j t)}$  changing thus its wavenumber and frequency according to

$$q_0 \rightarrow q_0 + jq_m \quad \text{and} \quad \omega_0 \rightarrow \omega_0 + j\omega_m \quad (3.36)$$

and amplifying or weakening its amplitude by a factor  $C$ . By contrast, a wave  $V^0 \psi_{\omega_0} e^{i(-q_0 x - \omega_0 t)}$  incident in the opposite direction is simply transmitted unaltered as  $(-q_0, \omega_0)$  would be an uncoupled mode.

In conclusion, by tuning  $q_m$  and  $\omega_m$  and using a modulated metamaterial, it is possible to realize a selective and directional wave converter/amplifier. To qualitatively illustrate the tuning potential of the wave mode conversion phenomenon, figure 6 shows how the normalized conversion distance  $Qd$  and the inverse amplification factor  $1/|C|$  vary in the mode space (level sets). For a given input mode  $(q_0, \omega_0)$  (marked with a black cross), the possible output modes  $(q_j, \omega_j)$  are distributed along the dispersion curve of the non-modulated medium (yellow solid lines). To each choice of output mode, there correspond a value of  $d$  and a value of  $C$  which can be read from the diagram. In the figure, the material constants of the metamaterial are such that  $M/m = 1$  and  $\delta_j k/k = 0.1$  and the input mode is  $(0.81Q, 0.525\Omega)$ . It appears then that the closer the output frequency is to the resonance frequency, the shorter  $d$  is and the higher  $C$  is. Therefore, for sensing applications, it seems appropriate to choose  $q_m$  and  $\omega_m$  such that the output frequency  $\omega_j$  falls in the vicinity of the resonance frequency  $\Omega$ . In this manner, a weak signal of frequency  $\omega_0$  overwhelmed by ambient noise can be amplified and converted into an almost resonant signal of frequency  $\Omega$ . Note that conversion is possible for both acoustic and optical modes, and it is further possible to switch between them by appropriately choosing  $q_m$  and  $\omega_m$ .

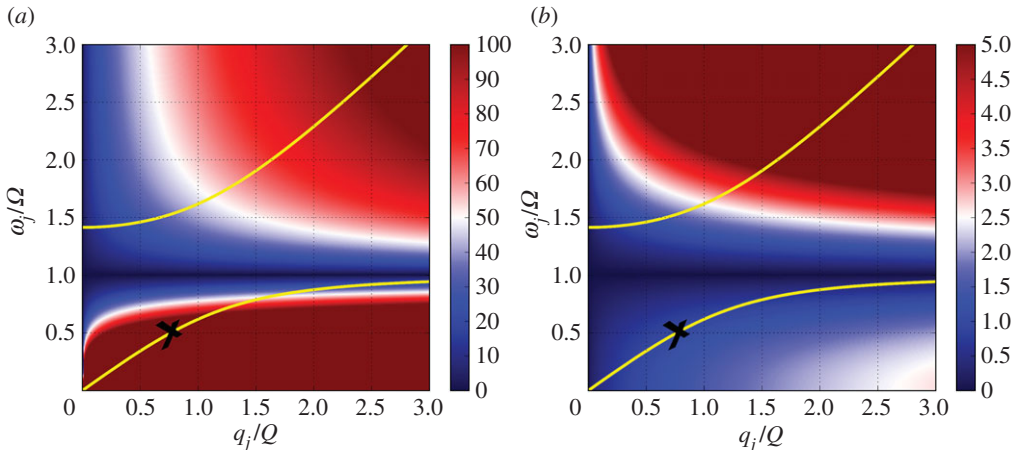


**Figure 6.** Variations (a) of the normalized conversion length  $Qd$  and (b) of the inverted amplification factor  $1/|C|$  as functions of the output mode  $(q_j, \omega_j)$  for a given input mode  $(q_0, \omega_0)$ . The crosses mark the input mode. (Online version in colour.)

### (f) Directional wave reflection

In the alternative scenario where  $q_0$  and  $q_j$  have opposite signs (e.g. pairs A and C in figure 5), expression (3.31) implies that the wavenumber changes  $\delta q_{\pm}$  in the vicinity of  $\delta\omega = 0$  are

$$\begin{aligned} \delta q_{\pm} &= \frac{\delta\omega}{2} \left( \frac{1}{c_0} + \frac{1}{c_j} \right) \\ &\pm i \sqrt{\left( \frac{1}{|q_0 q_j|} \left( \frac{|\delta_j k| m^2 \omega_0^2 \omega_j^2}{E(k - m\omega_0^2)(k - m\omega_j^2)} \right)^2 - \left( \frac{\delta\omega}{2} \left( \frac{1}{c_0} - \frac{1}{c_j} \right) \right)^2 \right)} = \delta q_b \pm i\delta q_c. \end{aligned}$$

These are complex valued in the neighbourhood of  $\delta\omega = 0$ , specifically for the range

$$|\delta\omega| < \frac{2|\delta_j k| m^2 \omega_0^2 \omega_j^2}{|q_0 q_j|^{1/2} E(k - m\omega_0^2)(k - m\omega_j^2)} \left| \frac{1}{c_0} - \frac{1}{c_j} \right|^{-1}. \quad (3.37)$$

Therefore, the field  $\tilde{\Psi}$  is composed of two damped waves of frequencies  $\omega_0$  and  $\omega_j$  and of complex wavenumbers  $\tilde{q}_0 = q_0 + \delta q$  and  $\tilde{q}_j = q_j + \delta q$ , respectively, where the complex first-order correction  $\delta q$  is given above and is due to the wave-like modulation.

The solution for the mode  $(q_0, \omega_0)$  incident from  $x < 0$  is, for  $x > 0$ ,

$$\psi(x, t) = V^0 e^{-\delta q_c x} (\Psi_\omega e^{i(q_0 x - \omega_0 t)} + C_+ \Psi_{\omega_j} e^{i(q_j x - \omega_j t)}) e^{i(\delta q_b x - \delta\omega t)}. \quad (3.38)$$

Consequently, within this frequency bandwidth centered on  $\omega_0$ , an incident wave of frequency  $\omega_0 + \delta\omega$  in the direction  $q_0$  only penetrates into the modulated metamaterial for a distance of the order of  $1/|\delta q_c|$  and is then reflected into a wave of frequency  $\omega_j$  going in the direction  $q_j$  opposite to  $q_0$ . The wave-like modulation thus opens locally a couple of directional bandgaps around the coupled eigenmodes  $(q_0, \omega_0)$  and  $(q_j, \omega_j)$  (see subplots (A) and (C) of figure 5).

### (g) Numerical simulations of non-reciprocal conversion and reflection

It is of interest to illustrate through direct numerical simulations the non-reciprocal behaviour of the modulated metamaterial characterized analytically so far. Specifically, we compute the transient response of the mass-in-mass lattice subject to various excitations and analyse its displacement field. Computations are performed thanks to a home-made finite difference code.

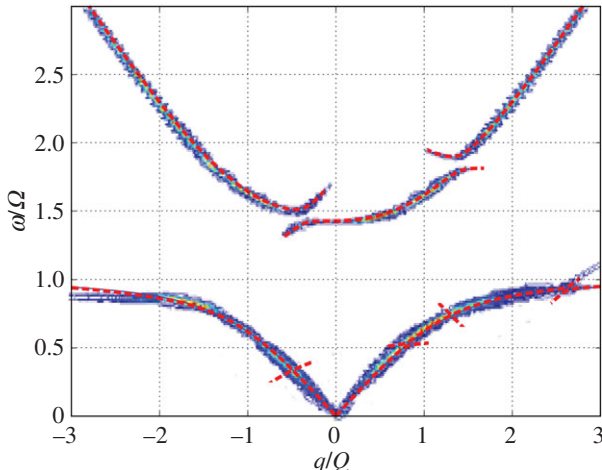


**Figure 7.** The dispersion curve of a modulated metamaterial obtained numerically (level sets) compared to the one determined analytically (dashed lines). (Online version in colour.)

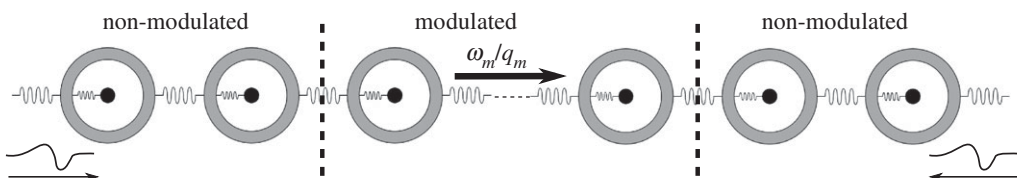


**Figure 8.** Set-up for the numerical testing of non-reciprocity: a modulated portion of the metamaterial serves as a transmitter between two non-modulated portions.

The constitutive and modulation parameters that we used are such that  $m/M=1$ ,  $q_m/Q=1.8$ ,  $\omega_m/\Omega=0.4$  and  $\delta_j k/k=0.1$ . These values are enough to characterize the non-dimensional response of the modulated metamaterial and can be completed by any particular set of parameters specifying  $m$ ,  $K$ ,  $k$  and  $\ell$  as long as scale separation is enforced through  $\Omega \ll 2\sqrt{K/M}$ .

First, we considered a modulated metamaterial lattice containing 3000 mass-in-mass unit cells placed in a whole circle so as to simulate periodic boundary conditions. The excitation was a broad-band tone burst displacement imposed at one of the outer masses. The imposed displacement has the form  $A_0(H(t) - H(t - N/f_c))(1 - \cos(\omega_c t/N))\sin(\omega_c t)$ , where  $A_0$  is an amplitude,  $f_c = \omega_c/2\pi$  is the central frequency,  $H$  is the Heaviside function and  $N$  is the number of cycles. The ensuing displacements at all positions and times  $u(x, t)$  are Fourier-analysed in space and time in order to obtain  $U_{q,\omega}$  whose amplitude is plotted as level sets over the  $(q, \omega)$ -plane and giving rise to the dispersion curve (figure 7). Numerical results are shown to agree with our analytical predictions. Note that we had to use different central frequencies  $f_c$  in order to cover the whole frequency range of interest with an acceptable accuracy, the plot of figure 7 being the superposition of all of these intermediary results.

Then, to test for non-reciprocal wave reflection and conversion at pairs  $A$  and  $B$ , respectively, a modulated portion of the metamaterial (1000 unit cells) is placed between two non-modulated ones (figure 8). The excitation is once again an imposed tone-burst-shaped displacement but with a much narrower spectrum (i.e. high number of cycles  $N$ ) and is applied once at the left end and once at the right end as illustrated. Figures 9 and 10 compare plots of incident, transmitted and reflected waves and, respectively, demonstrate numerically the phenomenon of non-reciprocal reflection/conversion predicted for pair  $A$  and of non-reciprocal transmission/conversion for pair  $B$ .

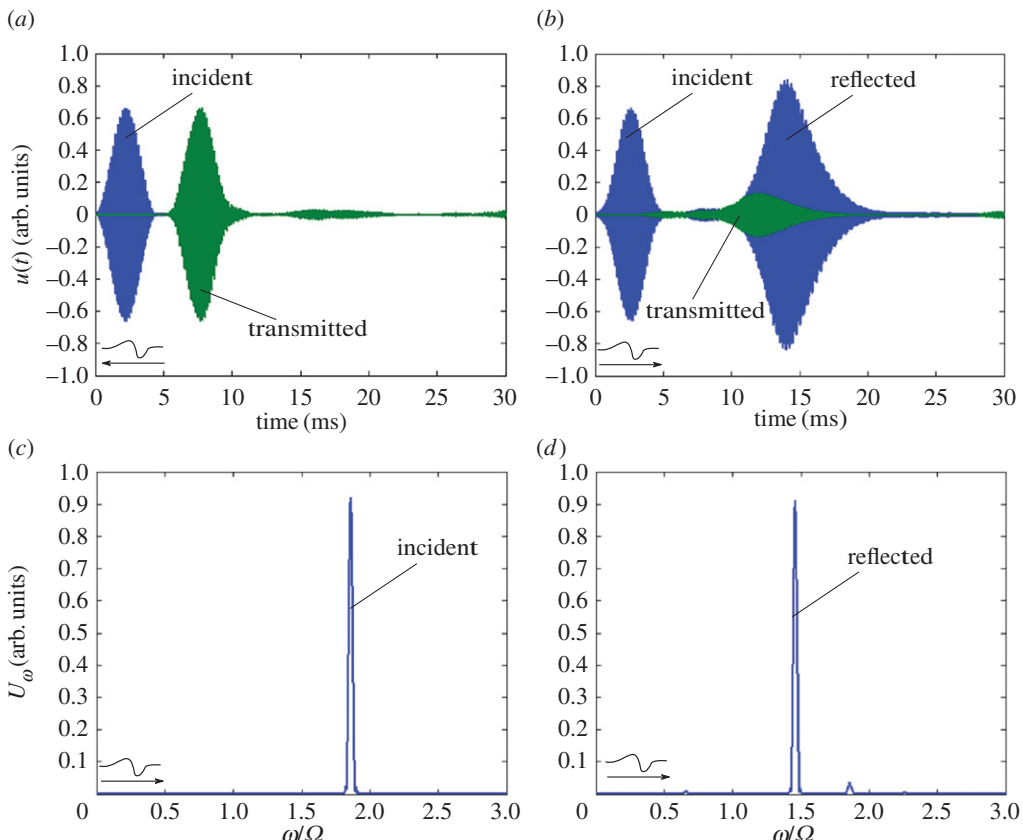


**Figure 9.** Plots of transient responses  $u(t)$  demonstrating non-reciprocal reflection/conversion of waves in a modulated metamaterial. On (a), a left-going incident wave of central frequency  $\omega \approx 1.8\Omega$  is transmitted unaltered if not for dispersive effects. On (b), the same wave incident to the right is almost entirely reflected, slightly amplified and its frequency shifted to  $\omega \approx 1.5\Omega$ . In the latter case, frequency spectra of incident and reflected waves are shown on (c) and (d), respectively. (Online version in colour.)

## 4. Short-wavelength modulations

In this section, we investigate a family of short-wavelength modulations for which  $q_m$  is much larger than the wavenumber of the propagating wave but remains small compared with the characteristic wavenumber  $2\pi/\ell$  so that (2.2) remains valid. The hypothesis on the amplitude of the modulation is relaxed on the other hand. The motion of the resonators will be described by a Hill's equation and will give rise to Bragg scattering phenomena but in time rather than in space. Even though non-reciprocity disappears in this short-wavelength regime, the modulated metamaterial remains a playground for phenomena that have no counterpart in non-modulated metamaterials as it features a non-standard effective mass density.

### (a) Homogenization

Our starting point is the equations of motion (2.2) with  $k = \tilde{k}(x, t)$  modulated. Following the methods of homogenization theory, the variations of  $u$  and  $v$  over space and time are split into two slow variations over  $x$  and  $t$  and one fast over  $\xi = q_m x - \omega_m t$  as in

$$u(x, t) = u(x, q_m x - \omega_m t, t) \quad \text{and} \quad v(x, t) = v(x, q_m x - \omega_m t, t), \quad (4.1)$$

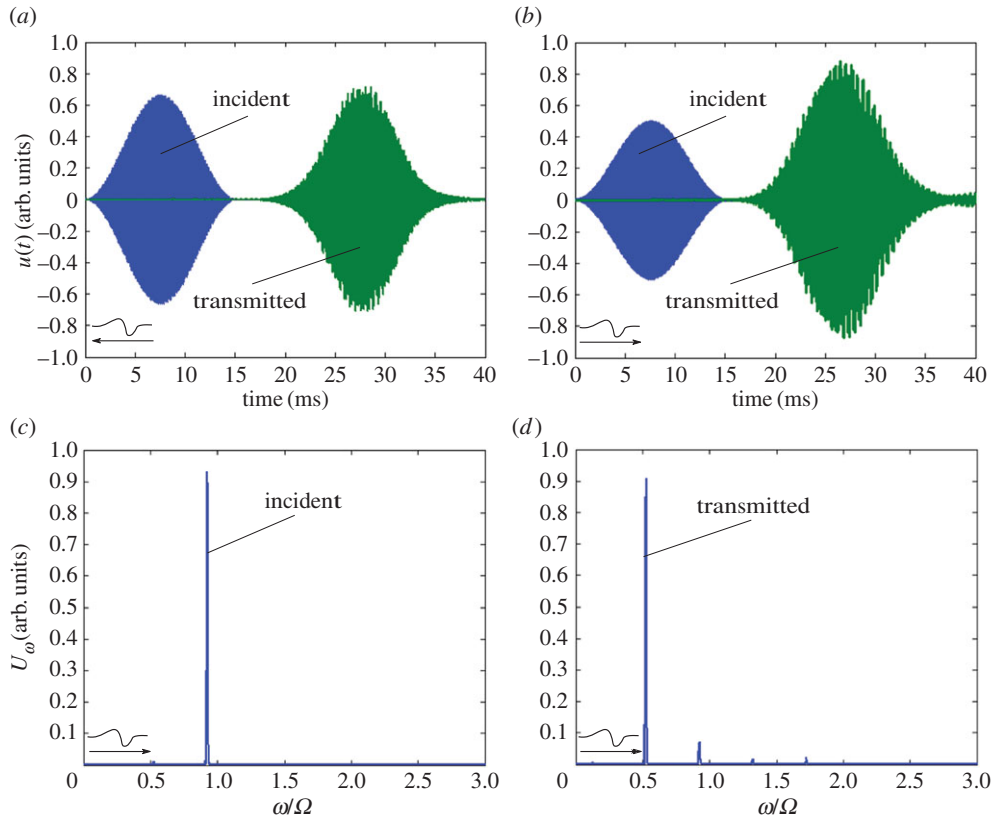


**Figure 10.** Plots of transient responses  $u(t)$  demonstrating non-reciprocal reflection/conversion of waves in a modulated metamaterial. On (a), a left-going incident wave of central frequency  $\omega \approx 1.8\Omega$  is transmitted unaltered if not for dispersive effects. On (b), the same wave incident to the right is almost entirely reflected, slightly amplified and its frequency shifted to  $\omega \approx 1.5\Omega$ . In the latter case, frequency spectra of incident and reflected waves are shown on (c) and (d), respectively. (Online version in colour.)

where  $u(x, \xi, t)$  and  $v(x, \xi, t)$  are solutions to the two-scale motion equations

$$\left. \begin{aligned} M(\partial_t - \omega_m \partial_\xi)^2 u &= -\tilde{k}(u - v) + E(\partial_x + \epsilon^{-1} q_m \partial_\xi)^2 u \\ m(\partial_t - \omega_m \partial_\xi)^2 v &= -\tilde{k}(v - u). \end{aligned} \right\} \quad (4.2)$$

and

Above, we have introduced a scaling parameter  $\epsilon$  taken to be infinitely small to account for the limit  $q_m \rightarrow \infty$ .

It is possible to assume that the unknown fields  $u$  and  $v$  have sinusoidal plane harmonic variations with respect to  $x$  and  $t$  of wavenumber  $q$  and frequency  $\omega$ , that is that they are Floquet–Bloch waves:

$$u(x, \xi, t) = U(\xi) e^{i(qx - \omega t)} \quad \text{and} \quad v(x, \xi, t) = V(\xi) e^{i(qx - \omega t)}. \quad (4.3)$$

Thus, in physical terms, our working hypothesis  $\epsilon \ll 1$  is equivalent to  $q \ll q_m$ . The periodic amplitudes  $U$  and  $V$  are next expanded into the asymptotic series

$$U = U^0 + \epsilon U^1 + \epsilon^2 U^2 + \dots \quad \text{and} \quad V = V^0 + \epsilon V^1 + \epsilon^2 V^2 + \dots \quad (4.4)$$

where  $U^n$  and  $V^n$  are corrections of order  $n$ . Note that we are only interested in obtaining the equations governing the leading-order amplitudes  $U^0$  and  $V^0$  as they describe the behaviour of a metamaterial subjected to a short-wavelength modulation.

Inserting the above expansions into the equations of motion (4.2), a hierarchy of motion equations is obtained. To the lowest order (in  $\epsilon^{-2}$ ), one has

$$0 = E\partial_\xi^2 U^0 \quad (4.5)$$

implying that  $U^0$  is a uniform amplitude, whereas  $V^0$  remains unknown so far. The first-order equations (in  $\epsilon^{-1}$ ) turn out to play no role and will not be detailed. The second-order equations (in  $\epsilon^0$ ) are

$$\left. \begin{aligned} -M\omega^2 U^0 &= -\tilde{k}(U^0 - V^0) - Eq^2 U^0 + \partial_\xi^2 U^2 \\ m(i\omega + \omega_m \partial_\xi)^2 V^0 &= -\tilde{k}(V^0 - U^0). \end{aligned} \right\} \quad (4.6)$$

and

It can be seen that the first of these equations involves the second-order correction  $U^2$ , whereas the second one is a leading-order equation governing  $U^0$  and  $V^0$ . By averaging the first equation and keeping the second one as it is, we obtain a couple of motion equations governing  $U^0$  and  $V^0$ ,

$$\left. \begin{aligned} -M\omega^2 U^0 &= -\langle k(U^0 - V^0) \rangle - Eq^2 U^0 \\ m(i\omega + \omega_m \partial_\xi)^2 V^0 &= -\tilde{k}(V^0 - U^0). \end{aligned} \right\} \quad (4.7)$$

and

Recall that  $U^0$  was proven uniform but  $V^0$  is generally  $\xi$ -dependent.

## (b) A series representation of the effective mass

Given that  $\omega_m \partial_\xi = -\partial_t$ , the resonators satisfy the forced Hill's equation

$$m(-i\omega + \partial_t)^2 V^0 = -\tilde{k}(V^0 - U^0), \quad (4.8)$$

where  $\tilde{k}U^0$  is seen as a periodic forcing term. We focus our attention on characterizing, if any, the resonance frequencies  $\Omega_{\text{eff}}$  of the resonators. This problem is similar to determining the dispersion curve resulting from Bragg scattering in a one-dimensional phononic crystal and has no analytical solutions, in general. Nonetheless, some interesting qualitative properties can still be inferred thanks to a series expansion of the effective mass operator.

Before doing so, a re-writing of Hill's equation will prove useful. So let  $T = 2\pi/\omega_m$  be the modulation period and  $\tau = t/T$  a non-dimensional time variable. The coupling  $\tilde{k}$  is therefore a 1-periodic function in  $\tau$  and the resonators equation can be recast into

$$m(-iv + \partial_\tau)^2 V^0 = -T^2 \tilde{k}(V^0 - U^0), \quad (4.9)$$

where  $v = T\omega$  is a non-dimensional frequency.

At a given  $v$ , let  $\phi_j(v)$ ,  $j \in \mathbb{N}$ , be the eigenstates of equation (4.9). Thus, to each  $\phi_j(v)$  there corresponds an eigenvalue  $T_j^2(v)$  such that

$$m(-iv + \partial_\tau)^2 \phi_j(v) = -T_j^2(v) \tilde{k} \phi_j(v). \quad (4.10)$$

In this manner, using standard modal analysis techniques, the periodic amplitude  $V^0$  can be expanded into the series

$$V^0 = \sum_{j \in \mathbb{N}} \langle \bar{\phi}_j(v) \tilde{k} V^0 \rangle \phi_j(v) = -T^2 \sum_{j \in \mathbb{N}} \frac{\langle \tilde{k} \bar{\phi}_j(v) \rangle \phi_j(v)}{T_j^2(v) - T^2} U^0, \quad (4.11)$$

where a bar indicates complex conjugation. Therefore, the coupling force has the expression

$$\langle \tilde{k}(U^0 - V^0) \rangle = \sum_{j \in \mathbb{N}} \frac{T_j^2(v)}{T_j^2(v) - T^2} \left| \langle \tilde{k} \phi_j(v) \rangle \right|^2 U^0. \quad (4.12)$$

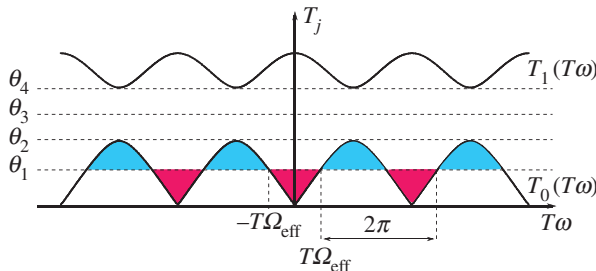


**Figure 11.** The first two branches of a typical dispersion curve associated with Hill's equation (4.9). (Online version in colour.)

As a result, the effective mass density takes the form

$$M_{\text{eff}}(\nu) = M + m \sum_{j \in \mathbb{N}} \frac{T^2}{T^2 - T_j^2(\nu)} |\langle \tilde{k} \phi_j(\nu) \rangle \langle \phi_j(\nu) \rangle|, \quad (4.13)$$

or, as a function of the frequency  $\omega$  and the modulation period  $T$ ,

$$M_{\text{eff}}(\omega, T) = M + m \sum_{j \in \mathbb{N}} \frac{T^2}{T^2 - T_j^2(T\omega)} |\langle \tilde{k} \phi_j(T\omega) \rangle \langle \phi_j(T\omega) \rangle|. \quad (4.14)$$

### (c) General properties of the effective mass density

Even though a closed-form expression is not available, the foregoing series expansion of the effective mass density operator is quite informative. First of all, the resonance frequencies  $\Omega_{\text{eff}}$  are solutions  $\omega$  to the equation

$$T_j^2(T\omega) - T^2 = 0. \quad (4.15)$$

The first two solution branches  $T_0$  and  $T_1$  are sketched in figure 11. Depending on the value of  $T$ , the effective mass density will exhibit or lack resonances.

- (i) When the above equation has a solution  $\Omega_{\text{eff}}(T)$ , it means that  $T$  falls into a<sup>1</sup> ‘passing band’ of Hill’s equation. In this case, by Floquet–Bloch theory, all the frequencies  $\pm\Omega_{\text{eff}}(T) + (2\pi/T)\mathbb{Z}$  are equally solutions, i.e. are equally resonance frequencies. An example is plotted in figure 11 where the line  $T = \theta_1$  intersects the first ‘passing band’  $T_0$  at regularly spaced points with a step of  $2\pi/T$ . The effective mass density will diverge at each of these intersections.
- (ii) When the above equation has no solutions,  $T$  falls within a ‘stopping band’ of Hill’s equation. In this case, no frequency  $\omega$  will make the inner masses resonate. An example is given in figure 11 where the line  $T = \theta_3$  does not intersect any of the branches  $T_j$ .

In both cases, however, the existence of bandgaps in the dispersion diagram of the hosting metamaterial is neither confirmed nor denied. In fact, the derived expression of the effective mass density operator, resulting from time-domain scattering, is genuinely different from the one usually obtained in non-modulated metamaterials (compare for instance with the expressions provided by Auriault & Bonnet [38] and by Milton *et al.* [4]). It turns out that the modulated metamaterial will sometimes exhibit non-resonating bandgaps, reminiscent of damped resonances, or, more surprisingly, will exhibit non-gapping resonances. More details are given subsequently.

To start with, recall that the effective mass density operator will remain finite away from resonance frequencies and will diverge near them to  $\pm\infty$ . The sign of the blow-up can be

<sup>1</sup>Quotation marks are used here to underline that we are referring to the band structure of Hill’s equation describing the resonators and not the band structure of the host metamaterial.

determined thanks to the following considerations. When  $T$  is in the  $n$ th passing band,  $T_n^2(T\omega) - T^2$  changes sign only at resonance frequencies. For instance, in figure 11, for  $T = \theta_1$ ,  $T_0^2(T\omega) - T^2$  alternates signs at each intersection (it is positive over the blue filled regions and negative over the red ones). Therefore, when  $\omega$  goes from one resonance frequency to the next, the denominator  $T_0^2(T\omega) - T^2$  will vanish from the same side (positive or negative) twice in a row and will make the effective mass density diverge towards the same infinity twice in a row as well. This marks another fundamental difference with the effective mass density of non-modulated metamaterials which, between two resonance frequencies, systematically goes from  $-\infty$  to  $+\infty$ .

More accurately, the above reasoning needs to be adjusted in the limiting case where  $T_n^2(T\omega) - T^2$  vanishes but does not change sign. This happens when the level of  $T$  is tangent from above or from below to a branch  $T_j$ . For instance, in figure 11,  $T = \theta_2$  is tangent from above to  $T_0$  so that  $T_0^2(T\omega) - T^2$  remains non-positive. Conversely,  $T = \theta_4$  is tangent from below to  $T_1$  and  $T_1^2(T\omega) - T^2$  stays non-negative. In these cases, the effective mass density diverges to the same infinity when  $\omega$  approaches any resonance frequency by increasing or decreasing values.

In summary, the series of infinities visited by  $M_{\text{eff}}$ , for increasing positive  $\omega$ , alternates periodically following the pattern  $(+--)$  or  $(-++-)$  except at the very end of a passing band where the pattern changes into  $(+++)$  and at the very beginning of a new passing band in which case the pattern is  $(---)$ . Hereafter, these patterns are referred to as *signatures*. Recall that the signature of a non-modulated metamaterial with multiple resonances is necessarily  $(+-+)$ .

Last, note that for infinitely small  $T$  unique values of the resonance frequency  $\Omega_{\text{eff}}(T) \xrightarrow[T \rightarrow 0]{} \Omega_{\text{eff}}$  and mass  $M_{\text{eff}}(\omega, T) \xrightarrow[T \rightarrow 0]{} M_{\text{eff}}$  are observed, where

$$\Omega_{\text{eff}} = \sqrt{\frac{\langle k \rangle}{m}} \quad \text{and} \quad M_{\text{eff}} = M + m \frac{\Omega_{\text{eff}}^2}{\Omega_{\text{eff}}^2 - \omega^2}. \quad (4.16)$$

The example described next, where a closed-form analytical expression of  $M_{\text{eff}}$  is available, will help appreciate the general properties presented in this subsection and illustrate new phenomena that have no counterpart in non-modulated inner-resonant metamaterials.

#### (d) Example: a high-amplitude modulation

A fairly simple closed-form analytical solution for Hill's equation can be obtained when the coupling stiffness  $\tilde{k}$  is a 'Dirac comb' as in

$$\Omega^2(t) = \frac{\tilde{k}(t)}{m} = \alpha + T\beta \sum_{j \in \mathbb{Z}} \delta(t - jT), \quad (4.17)$$

where  $\delta$  is the Dirac function. Though experimentally challenging, such modulation can be achieved in theory by letting  $\tilde{k}$  take a first positive value,  $k = m\alpha$ , over a period of time equal to  $T - \Delta t$  and then another positive value,  $k + \delta k = m(\alpha + T\beta/\Delta t)$ , over a period of  $\Delta t$ , for as small  $\Delta t$  as possible (figure 12). The considered modulation has therefore a very high amplitude.

The analytical advantage of Dirac combs is that they have particularly simple Fourier coefficients. For instance, those of  $\Omega^2$  are  $\Omega_0^2 = \alpha + \beta$ ,  $\Omega_{\eta \neq 0}^2 = \beta$ , where the Fourier variable  $\eta$  spans  $(2\pi/T)\mathbb{Z}$ . Taking this and the fact that  $U^0$  is uniform into account, expansion of equation (4.8) yields

$$-(\omega + \eta)^2 V_\eta = -\alpha V_\eta - \beta \sum_{\eta'} V_{\eta'} + \alpha U \delta_{n0} + \beta U, \quad (4.18)$$

where superscripts have been dropped to simplify notations. Summing the coefficients  $V_\eta$  over all  $\eta$  leads to

$$\sum_{\eta'} V_{\eta'} = \left( 1 + \frac{\omega^2}{\alpha - \omega^2 + \beta g(\omega, T)} \right) U, \quad (4.19)$$

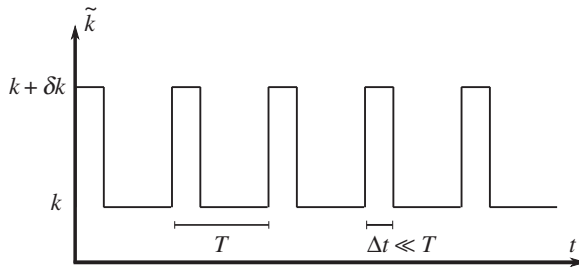


**Figure 12.** A high-amplitude modulation.

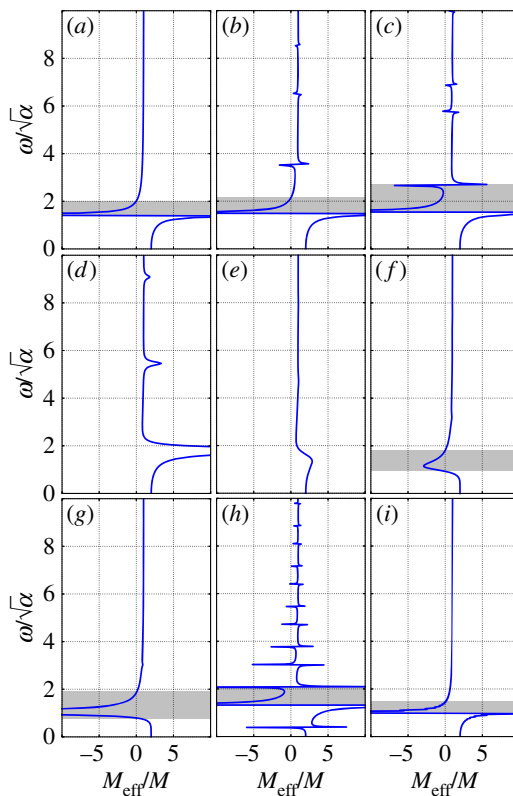


**Figure 13.** The profile of the normalized effective mass density  $M_{\text{eff}}/M$  as a function of the normalized frequency  $\omega/\sqrt{\alpha}$  for various values of  $T\sqrt{\alpha} = 0.1; 1.25; 1.49; 1.73; 2.01; 2.96; 3.12; 3.71; 100$  (*a*–*i*, in order). The fundamental bandgap is shaded. The properties of the corresponding metamaterial are such that  $M = m$  and  $\alpha = \beta$ . (Online version in colour.)

where

$$g(\omega, T) = \sum_{\eta} \frac{\alpha - \omega^2}{\alpha - (\omega + \eta)^2} = \frac{(\alpha - \omega^2)T\sqrt{\alpha} \sin(T\sqrt{\alpha})}{2\alpha(\cos(T\omega) - \cos(T\sqrt{\alpha}))}. \quad (4.20)$$

This allows us to conclude that the coupling force is

$$\langle k(U - V) \rangle = -\frac{m\omega^2}{\alpha - \omega^2} \left( \alpha - \frac{\beta\omega^2}{\alpha - \omega^2 + \beta g(\omega, T)} \right) U, \quad (4.21)$$

and that the effective mass can be expressed as

$$M_{\text{eff}}(\omega, T) = M + \frac{m\alpha}{\alpha - \omega^2} \left( \alpha - \frac{\beta\omega^2}{\alpha - \omega^2 + \beta g(\omega, T)} \right). \quad (4.22)$$

This closed-form expression of  $M_{\text{eff}}$  was used to generate the plots of figure 13. Values of  $T$  were chosen to illustrate different phenomena predicted by the general considerations of the previous subsection. On (a), the standard profile for a high-frequency short-wavelength modulation is plotted. On (b), multiple resonances with a signature  $(+ - - +)$  appear. Unlike the signature  $(+ - + -)$  of non-modulated metamaterials, the signature  $(+ - - +)$  does not obstruct bandgaps merging (c). Non-gaping resonances appear on (d) as  $T$  leaves the first ‘passing band’. Resonances disappear on (e) where  $T$  is now in the first ‘stopping band’. Plot (f) demonstrates the possibility of non-resonating bandgaps. A bandgap which extends to both sides of a resonance frequency is illustrated on (g). As  $T$  enters the second ‘passing band’, the signature is inverted into  $(- + + -)$  and resonances become denser because the step  $2\pi/T$  keeps decreasing as it is seen on (h). Last, on (i), for infinitely large  $T$ , the metamaterial is no longer modulated and a standard profile is recovered. In comparison to figure 11, plots (a,b,c) correspond to values similar to  $T = \theta_1$ , plot (d) to  $T = \theta_2$ , plots (e,f) to  $T = \theta_3$ , plot (g) to  $T = \theta_4$  and plots (h,i) to higher values of  $T$ .

The configurations sketched in figure 13c,g are of particular interest as they feature unusually broad bandgaps almost twice as wide as the bandgap that the non-modulated metamaterial exhibits on plot (i). Note finally that in some frequency domains, Hill’s equation is known to feature instabilities that should be avoided for the above results to be fully useful [1].

## 5. Conclusion

Qualitatively, within a weakly modulated medium, travelling and pump waves interact only when a phase-matching condition is satisfied. If so, the incident wave will be scattered by the pump wave. When the incident and scattered waves propagate in the same direction, we speak of ‘veering’: the incident wave is converted into a transmitted wave with a shifted frequency. Otherwise, the incident wave is fully reflected, a phenomenon called ‘locking’. Note that veering can only occur in dispersive media, whereas locking occurs in both dispersive and non-dispersive media. The modulated metamaterial considered in this paper was shown to feature both effects.

The asymmetric nature of the phase matching condition immediately implies that the interaction between travelling and pump waves is directional. Thus, waves that are either converted or reflected when incident in one direction are simply transmitted unaltered if incident in the opposite direction. The amplification factor and characteristic length of these one-way phenomena turned out to be tunable as well thanks to the dispersive nature of the host metamaterial.

Furthermore, beyond non-reciprocal effects, strong space–time modulations have a significant impact on the behaviour of the effective mass operator in the homogenization limit. As a matter of fact, in addition to the main bandgap of the inner-resonant structure, a set of low-frequency time-domain-Bragg-scattering bandgaps was observed. Most importantly, in contrast with non-modulated metamaterials, these new modulation-induced bandgaps were shown to be able to merge.

Modulating the resonance frequency of an inner resonant metamaterial so as to break time-reversal symmetry and reciprocity or to generate new non-standard effective mass operators offers a promising potential in the field of wave control in general and in one-way conversion/amplification in particular.

**Data accessibility.** This paper does not have any experimental data.

**Authors’ contributions.** H.N. and G.H. conceived the core concepts and mathematical model. H.N., A.N. and G.H. derived and interpreted the analytical results. H.C. and H.N. carried the numerical simulations. G.H., A.N. and M.H. supervised the modelling and simulation. All authors discussed the results, commented on the manuscript and approved it.

**Competing interests.** The authors have no competing interests.

**Funding.** This work is supported by the Air Force Office of Scientific Research under grant no. AF 9550-15-1-0016 with Program Manager Dr Byung-Lip (Les) Lee and the NSF EFRI under award no. 1641078.

## References

- Brillouin L. 1953 *Wave propagation in periodic structures: electric filters and crystal lattices*. Dover Phoenix Editions. New York, NY: Dover Publications.
- Liu Z, Zhang X, Mao Y, Zhu YY, Yang Z, Chan CT, Sheng P. 2000 Locally resonant sonic materials. *Science* **289**, 1734–1736. ([doi:10.1126/science.289.5485.1734](https://doi.org/10.1126/science.289.5485.1734))
- Li J, Chan CT. 2004 Double-negative acoustic metamaterial. *Phys. Rev. E* **70**, 055602. ([doi:10.1103/PhysRevE.70.055602](https://doi.org/10.1103/PhysRevE.70.055602))
- Milton GW, Briane M, Willis JR. 2006 On cloaking for elasticity and physical equations with a transformation invariant form. *New J. Phys.* **8**, 248–267. ([doi:10.1088/1367-2630/8/10/248](https://doi.org/10.1088/1367-2630/8/10/248))
- Ding Y, Liu Z, Qiu C, Shi J. 2007 Metamaterial with simultaneously negative bulk modulus and mass density. *Phys. Rev. Lett.* **99**, 093904. ([doi:10.1103/PhysRevLett.99.093904](https://doi.org/10.1103/PhysRevLett.99.093904))
- Yao S, Zhou X, Hu GK. 2008 Experimental study on negative effective mass in a 1D mass-spring system. *New J. Phys.* **10**, 043020. ([doi:10.1088/1367-2630/10/4/043020](https://doi.org/10.1088/1367-2630/10/4/043020))
- Auriault JL, Boutin C. 2012 Long wavelength inner-resonance cut-off frequencies in elastic composite materials. *Int. J. Solids Struct.* **49**, 3269–3281. ([doi:10.1016/j.ijsolstr.2012.07.002](https://doi.org/10.1016/j.ijsolstr.2012.07.002))
- Zhu R, Liu XN, Hu GK, Sun CT, Huang GL. 2014 Negative refraction of elastic waves at the deep-subwavelength scale in a single-phase metamaterial. *Nat. Commun.* **5**, 5510. ([doi:10.1038/ncomms6510](https://doi.org/10.1038/ncomms6510))
- Yu Z, Fan S. 2009 Complete optical isolation created by indirect interband photonic transitions. *Nat. Photonics* **3**, 91–94. ([doi:10.1038/nphoton.2008.273](https://doi.org/10.1038/nphoton.2008.273))
- Zanjani MB, Davoyan AR, Mahmoud AM, Engheta N, Lukes JR. 2014 One-way phonon isolation in acoustic waveguides. *Appl. Phys. Lett.* **104**, 081905. ([doi:10.1063/1.4866590](https://doi.org/10.1063/1.4866590))
- Zanjani MB, Davoyan AR, Engheta N, Lukes JR. 2015 NEMS with broken T symmetry: graphene based unidirectional acoustic transmission lines. *Sci. Rep.* **5**, 09926. ([doi:10.1038/srep09926](https://doi.org/10.1038/srep09926))
- Fleury R, Sounas DL, Sieck CF, Haberman MR, Alù A. 2014 Sound isolation and giant linear nonreciprocity in a compact acoustic circulator. *Science* **343**, 516–519. ([doi:10.1126/science.1246957](https://doi.org/10.1126/science.1246957))
- Swinteck N, Matsuo S, Runge K, Vasseur JO, Lucas P, Deymier PA. 2015 Bulk elastic waves with unidirectional backscattering-immune topological states in a time-dependent superlattice. *J. Appl. Phys.* **118**, 063103. ([doi:10.1063/1.4928619](https://doi.org/10.1063/1.4928619))
- Trainiti G, Ruzzene M. 2016 Non-reciprocal elastic wave propagation in spatiotemporal periodic structures. *New J. Phys.* **18**, 083047. ([doi:10.1088/1367-2630/18/8/083047](https://doi.org/10.1088/1367-2630/18/8/083047))
- Nassar H, Xu XC, Norris AN, Huang GL. 2017 Modulated phononic crystals: Non-reciprocal wave propagation and Willis materials. *J. Mech. Phys. Solids* **101**, 10–29. ([doi:10.1016/j.jmps.2017.01.010](https://doi.org/10.1016/j.jmps.2017.01.010))
- Liang B, Yuan B, Cheng JC. 2009 Acoustic diode: Rectification of acoustic energy flux in one-dimensional systems. *Phys. Rev. Lett.* **103**, 104301. ([doi:10.1103/PhysRevLett.103.104301](https://doi.org/10.1103/PhysRevLett.103.104301))
- Mousavi SH, Khanikaev AB, Wang Z. 2015 Topologically protected elastic waves in phononic metamaterials. *Nat. Commun.* **6**, 8682. ([doi:10.1038/ncomms9682](https://doi.org/10.1038/ncomms9682))
- Lu J, Qiu C, Ke M, Liu Z. 2016 Valley vortex states in sonic crystals. *Phys. Rev. Lett.* **116**, 093901. ([doi:10.1103/PhysRevLett.116.093901](https://doi.org/10.1103/PhysRevLett.116.093901))
- Lu J, Qiu C, Ye L, Fan X, Ke M, Zhang F, Liu Z. 2016 Observation of topological valley transport of sound in sonic crystals. *Nat. Phys.* **13**, 369–374. ([doi:10.1038/nphys3999](https://doi.org/10.1038/nphys3999))
- Fleury R, Sounas DL, Haberman MR, Alù A. 2015 Nonreciprocal acoustics. *Acoust. Today* **11**, 14–21.
- Khanikaev AB, Fleury R, Mousavi SH, Alù A. 2015 Topologically robust sound propagation in an angular-momentum-biased graphene-like resonator lattice. *Nat. Commun.* **6**, 8260. ([doi:10.1038/ncomms9260](https://doi.org/10.1038/ncomms9260))
- Yang Z, Gao F, Shi X, Lin X, Gao Z, Chong Y, Zhang B. 2015 Topological acoustics. *Phys. Rev. Lett.* **114**, 114301. ([doi:10.1103/PhysRevLett.114.114301](https://doi.org/10.1103/PhysRevLett.114.114301))
- Chen ZG, Wu Y. 2016 Tunable topological phononic crystals. *Phys. Rev. Appl.* **5**, 054021. ([doi:10.1103/PhysRevApplied.5.054021](https://doi.org/10.1103/PhysRevApplied.5.054021))

24. Slater JC. 1958 Interaction of waves in crystals. *Rev. Mod. Phys.* **30**, 197–222. (doi:10.1103/RevModPhys.30.197)
25. Simon JC. 1960 Action of a progressive disturbance on a guided electromagnetic wave. *IRE Trans. Microw. Theory Tech.* **8**, 18–29. (doi:10.1109/TMTT.1960.1124657)
26. Louisell W. 1960 *Coupled mode and parametric electronics*. New York, NY: Wiley.
27. Hessel A, Oliner AA. 1961 Wave propagation in a medium with a progressive sinusoidal disturbance. *IRE Trans. Microw. Theory Tech.* **9**, 337–343. (doi:10.1109/TMTT.1961.1125340)
28. Cassedy ES, Oliner AA. 1963 Dispersion relations in time-space periodic media: Part I-stable interactions. *Proc. IEEE* **51**, 1342–1359. (doi:10.1109/PROC.1963.2566)
29. Cassedy ES, Oliner AA. 1963 Dispersion relations in time-space periodic media: Part II-unstable interactions. *Proc. IEEE* **51**, 1154–1168. (doi:10.1109/PROC.1963.2566)
30. Lurie KA. 2007 *An introduction to the mathematical theory of dynamic materials*. New York, NY: Springer.
31. Milton GW, Mattei O. 2017 Field patterns: a new mathematical object. *Proc. R. Soc. A* **473**, 20160819. (doi:10.1098/rspa.2016.0819)
32. Casadei F, Delpero T, Bergamini A, Ermanni P, Ruzzene M. 2012 Piezoelectric resonator arrays for tunable acoustic waveguides and metamaterials. *J. Appl. Phys.* **112**, 064902. (doi:10.1063/1.4752468)
33. Chen YY, Huang GL, Sun CT. 2014 Band gap control in an active elastic metamaterial with negative capacitance piezoelectric shunting. *J. Vib. Acoust.* **136**, 061008. (doi:10.1115/1.4028378)
34. Chen YY, Hu GK, Huang GL. 2016 An adaptive metamaterial beam with hybrid shunting circuits for extremely broadband control of flexural waves. *Smart Mater. Struct.* **25**, 105036. (doi:10.1088/0964-1726/25/10/105036)
35. Reed EJ, Soljačić M, Joannopoulos JD. 2003 Reversed Doppler effect in photonic crystals. *Phys. Rev. Lett.* **91**, 89–92. (doi:10.1103/PhysRevLett.91.133901)
36. Danas K, Kankanala SV, Triantafyllidis N. 2012 Experiments and modeling of iron-particle-filled magnetorheological elastomers. *J. Mech. Phys. Solids* **60**, 120–138. (doi:10.1016/j.jmps.2011.09.006)
37. Gump J, Finkler I, Xia H, Sooryakumar R, Bresser WJ, Boolchand P. 2004 Light-induced giant softening of network glasses observed near the mean-field rigidity transition. *Phys. Rev. Lett.* **92**, 245501. (doi:10.1103/PhysRevLett.92.245501)
38. Auriault JL, Bonnet G. 1985 Dynamics of periodic elastic composites (Dynamique des composites élastiques périodiques). *Arch. Mech. Stosow.* **37**, 269–284.
39. Huang HH, Sun CT, Huang GL. 2009 On the negative effective mass density in acoustic metamaterials. *Int. J. Eng. Sci.* **47**, 610–617. (doi:10.1016/j.ijengsci.2008.12.007)
40. Mace BR, Manconi E. 2012 Wave motion and dispersion phenomena: veering, locking and strong coupling effects. *J. Acoust. Soc. Am.* **131**, 1015–1028. (doi:10.1121/1.3672647)